



UNIVERSITY OF LEEDS

This is a repository copy of *Global Synthesis of Regional Holocene Hydroclimate Variability Using Proxy and Model Data*.

White Rose Research Online URL for this paper:

<https://eprints.whiterose.ac.uk/200726/>

Version: Published Version

---

**Article:**

Hancock, CL, McKay, NP, Erb, MP et al. (5 more authors) (2023) Global Synthesis of Regional Holocene Hydroclimate Variability Using Proxy and Model Data.

Paleoceanography and Paleoclimatology, 38 (6). e2022PA004597. ISSN 2572-4525

<https://doi.org/10.1029/2022pa004597>

---

© 2023. American Geophysical Union. Reproduced in accordance with the publisher's self-archiving policy.

**Reuse**

Items deposited in White Rose Research Online are protected by copyright, with all rights reserved unless indicated otherwise. They may be downloaded and/or printed for private study, or other acts as permitted by national copyright laws. The publisher or other rights holders may allow further reproduction and re-use of the full text version. This is indicated by the licence information on the White Rose Research Online record for the item.

**Takedown**

If you consider content in White Rose Research Online to be in breach of UK law, please notify us by emailing [eprints@whiterose.ac.uk](mailto:eprints@whiterose.ac.uk) including the URL of the record and the reason for the withdrawal request.



[eprints@whiterose.ac.uk](mailto:eprints@whiterose.ac.uk)  
<https://eprints.whiterose.ac.uk/>

# Paleoceanography and Paleoclimatology

## RESEARCH ARTICLE

10.1029/2022PA004597

### Key Points:

- Eight hundred thirteen proxy records characterize terrestrial Holocene hydroclimate. Results are compared to existing paleotemperature data and climate models
- Proxy records and models agree on the sign of the precipitation anomaly at 6 ka in 63% of the study regions compared to 26% for temperature
- Proxy-model hydroclimate agreement is highest for tropical monsoon regions. Proxies and models disagree about trends in North America

### Supporting Information:

Supporting Information may be found in the online version of this article.

### Correspondence to:

C. L. Hancock,  
[clh624@nau.edu](mailto:clh624@nau.edu)

### Citation:

Hancock, C. L., McKay, N. P., Erb, M. P., Kaufman, D. S., Routson, C. R., Ivanovic, R. F., et al. (2023). Global synthesis of regional Holocene hydroclimate variability using proxy and model data. *Paleoceanography and Paleoclimatology*, 38, e2022PA004597. <https://doi.org/10.1029/2022PA004597>

Received 11 DEC 2022  
Accepted 11 MAY 2023

### Author Contributions:

**Conceptualization:** Christopher L. Hancock, Nicholas P. McKay, Michael P. Erb, Darrell S. Kaufman, Cody R. Routson  
**Data curation:** Christopher L. Hancock, Nicholas P. McKay, Michael P. Erb  
**Formal analysis:** Christopher L. Hancock  
**Funding acquisition:** Nicholas P. McKay, Michael P. Erb  
**Investigation:** Christopher L. Hancock, Ruza F. Ivanovic, Lauren J. Gregoire, Paul Valdes  
**Methodology:** Christopher L. Hancock, Nicholas P. McKay, Michael P. Erb  
**Software:** Nicholas P. McKay  
**Validation:** Christopher L. Hancock  
**Visualization:** Christopher L. Hancock

## Global Synthesis of Regional Holocene Hydroclimate Variability Using Proxy and Model Data

Christopher L. Hancock<sup>1</sup> , Nicholas P. McKay<sup>1</sup> , Michael P. Erb<sup>1</sup> , Darrell S. Kaufman<sup>1</sup> , Cody R. Routson<sup>1</sup> , Ruza F. Ivanovic<sup>2</sup> , Lauren J. Gregoire<sup>2</sup> , and Paul Valdes<sup>3</sup>

<sup>1</sup>School of Earth and Sustainability, Northern Arizona University, Flagstaff, AZ, USA, <sup>2</sup>School of Earth and Environment, University of Leeds, Leeds, UK, <sup>3</sup>School of Geographical Sciences, University of Bristol, Bristol, UK

**Abstract** Substantial changes in terrestrial hydroclimate during the Holocene are recorded in geological archives and simulated by computer models. To identify spatial and temporal patterns during the past 12 ka, proxy records sensitive to changing precipitation and effective moisture (precipitation minus evaporation) were compiled from across the globe ( $n = 813$ ). Proxy composite timeseries were computed for 30 of the IPCC AR6 regions and compared to two full-Holocene transient model simulations (TraCE-21ka and HadCM3) and twelve mid-Holocene CMIP6 simulations. We find that throughout Northern Hemisphere monsoon regions, proxy and model simulations indicate wetter-than-modern conditions during the early and mid-Holocene while Southern Hemisphere monsoon regions were drier. This insolation driven trend toward modern values began approximately 6,000 years ago, and the clear agreement among proxy records and models may reflect the large magnitude of precipitation change and consistent atmospheric circulation forcing mechanism for these regions. In the midlatitudes, the pattern of change is less certain. Generally, proxy composites show a wetting trend throughout the Holocene for the northern midlatitudes, possibly due to strengthening westerlies from an increasing latitudinal temperature gradient. However, simulations indicate that the magnitude of change was relatively low, and for portions of North America, there is a proxy-model disagreement. At high latitudes, hydroclimate is positively correlated with temperature in both proxies and models, consistent with projected wetting as temperatures rise. Overall, this large proxy database reveals a coherent pattern of hydroclimate variability despite the challenges associated with reconstructing hydroclimate fields.

**Plain Language Summary** A new compilation of natural records of past climate (called “proxy records”) characterizes changes to precipitation and moisture conditions during the past 12,000 years. The spatial patterns of climate changes are examined regionally. We also compare the proxy records with climate model simulations to evaluate agreement between these independent data sources. Our results highlight a trend toward modern moisture conditions beginning approximately 6,000 years ago, when Northern Hemisphere monsoon regions in North Africa and Asia started to become dryer and Southern Hemisphere regions in South America and Africa became wetter. These shifts are explained by the seasonal distribution of sunlight associated with slow changes in Earth’s orbit. In the Northern Hemisphere midlatitudes, a wetting trend throughout the past 12,000 years is apparent in the proxy records. Changes in the distribution of temperatures may have influenced atmospheric circulation by strengthening winds and increasing moisture delivery to these midlatitude regions. In the polar regions, a covariance between precipitation and temperature are correlated in both models and proxy records. Because modern warming is concentrated on land and in the Arctic, our results provide a partial analogue for the impacts of future warming on hydroclimate.

## 1. Introduction

The Holocene (11.7 ka to present) is an important period for understanding the mechanisms underlying current and future climate variability. During this time, proxy data record significant and occasionally abrupt changes in regional precipitation amounts. For example, the African Humid Period (deMenocal et al., 2000; Tierney et al., 2017), a strengthened Asian Summer Monsoon (An et al., 2000; Cai et al., 2010; Jin et al., 2014), and aridity in North America (Bartlein et al., 1984; Shuman & Marsicek, 2016) are well-studied hydroclimatic anomalies during the early Holocene. However, the spatial extent, magnitude, and timing of these changes remain poorly constrained. Here, we compare proxies and models to better understand past changes and provide a partial analogue for the impacts of current and future warming on hydroclimate.

**Writing – original draft:** Christopher L. Hancock  
**Writing – review & editing:** Christopher L. Hancock, Nicholas P. McKay, Michael P. Erb, Darrell S. Kaufman, Cody R. Routson

To explain patterns of hydroclimate variability during the Holocene, researchers often invoke systematic changes in seasonal insolation due to changes in Earth's orbital precession and obliquity. During the early Holocene, more intense summertime insolation in the Northern Hemisphere shifted the Intertropical Convergence Zone (ITCZ) northward and strengthened monsoonal circulation across Asia and North Africa (COHMAP Members, 1988; Shi & Yan, 2019). This warming pattern also reduced the latitudinal thermal gradient (LTG), which may have weakened westerly circulation and decreased precipitation across Northern Hemisphere midlatitudes (Routson et al., 2019). Tropical and extratropical climates are dynamically linked as weakened westerly circulation is associated with a poleward expansion of monsoon systems (An et al., 2012; Chou & Neelin, 2003; Davis & Brewer, 2009; Kong & Chiang, 2020). A reversed pattern in the Southern Hemisphere reflects an opposite trend in summertime insolation intensity with intrahemispheric circulation connected through meridional migration of the ITCZ (H. Cheng et al., 2012; Deininger et al., 2020; Zhao & Harrison, 2012).

Significant questions remain regarding the evolution of hydroclimate during the Holocene. In part, this stems from the spatial heterogeneity of precipitation amount, type, and seasonality between different regions as well as the complex climate forcings that drive regional atmospheric circulation and local moisture variability (Shepherd, 2014; Williams et al., 2010). Furthermore, the limited geographic distribution of calibrated hydroclimate proxies and the general diversity of proxy types challenge comparisons among proxies and between proxy data and model simulations. As a result, quantitative global climate reconstructions of the past 12 ka primarily focus on global mean surface temperature (e.g., Kaufman, McKay, Routson, Erb, Davis, et al., 2020; Marcott et al., 2013; Osman et al., 2021). Otherwise, previous multi-region hydroclimate data compilations are commonly limited in scope to a specific time slice (e.g., Brierley et al., 2020; Tarasov et al., 1998) and/or a single proxy type (e.g., H. Cheng et al., 2012; Liefert & Shuman, 2020; Mauri et al., 2014). However, conclusions based on a small number of proxy records or a single archive type (e.g., speleothems, lake sediments, peat deposits, etc.) may not be reproduced across proxy types (J. Cheng et al., 2021; Lézine et al., 2011). Thus, a multi-proxy synthesis is needed to develop a comprehensive view of global Holocene hydroclimate variability.

Global climate models provide insight into dynamic processes, spatial patterns, and seasonalities, which proxy data are not always able to resolve. Transient simulations allow for investigation into the physical mechanisms forcing long-term trends (Bartlein et al., 1998; Shi & Yan, 2019), as well as comparisons between short-term events throughout the Holocene (e.g., Ning et al., 2019). Overall, the agreement between model and proxy data shows a similar direction of change for many regions (Jiang et al., 2015). However, model simulations may underestimate the amount of precipitation change (Lu et al., 2019; Morrill et al., 2019), the role of feedbacks related to vegetation or dust (Harrison et al., 2014), and the importance of atmospheric circulation modes on regional moisture delivery (Mauri et al., 2014). Furthermore, most proxy-model comparisons focus on mid-Holocene (6 ka) anomalies relative to present (e.g., Brierley et al., 2020; Chevalier et al., 2017; Lin et al., 2019), which limits analysis to a narrow time slice without the benefit of examining long-term trends and the impact of transient climate forcings.

Here, we present a new multi-proxy data set to investigate centennial- and millennial-scale terrestrial hydroclimate variability. The broad spatial distribution and diversity of proxy types provide a robust view of climate evolution during the Holocene. We assess spatial-temporal patterns of hydroclimate variability, examine agreement among proxy data, and evaluate climate model simulations. We focus on regional composites of proxy records to quantify the average signal among these data as well as the relative timing and direction of changes among regions. To quantify the level of agreement between proxy and model data we examine the sign of 6 ka anomalies (wetter or drier than preindustrial) and contrast this metric with those for temperatures. We also examine patterns of covariance between precipitation and temperature, both in proxy data and in model simulations.

## 2. Materials and Methods

### 2.1. Proxy Data

The compilation, metadata standardization, and publication of a new Holocene hydroclimate multi-proxy data set represents a significant product of this research project (Figure 1). Records ( $n = 813$ ) originate from a variety of previous compilations that concentrate on either a specific geographic region or proxy type. We supplemented these compilations with additional data available on repositories such as PANGAEA or NCDC. Only records interpreted by the original author(s) as reflecting either precipitation amount (P) ( $n = 508$ ) or effective moisture

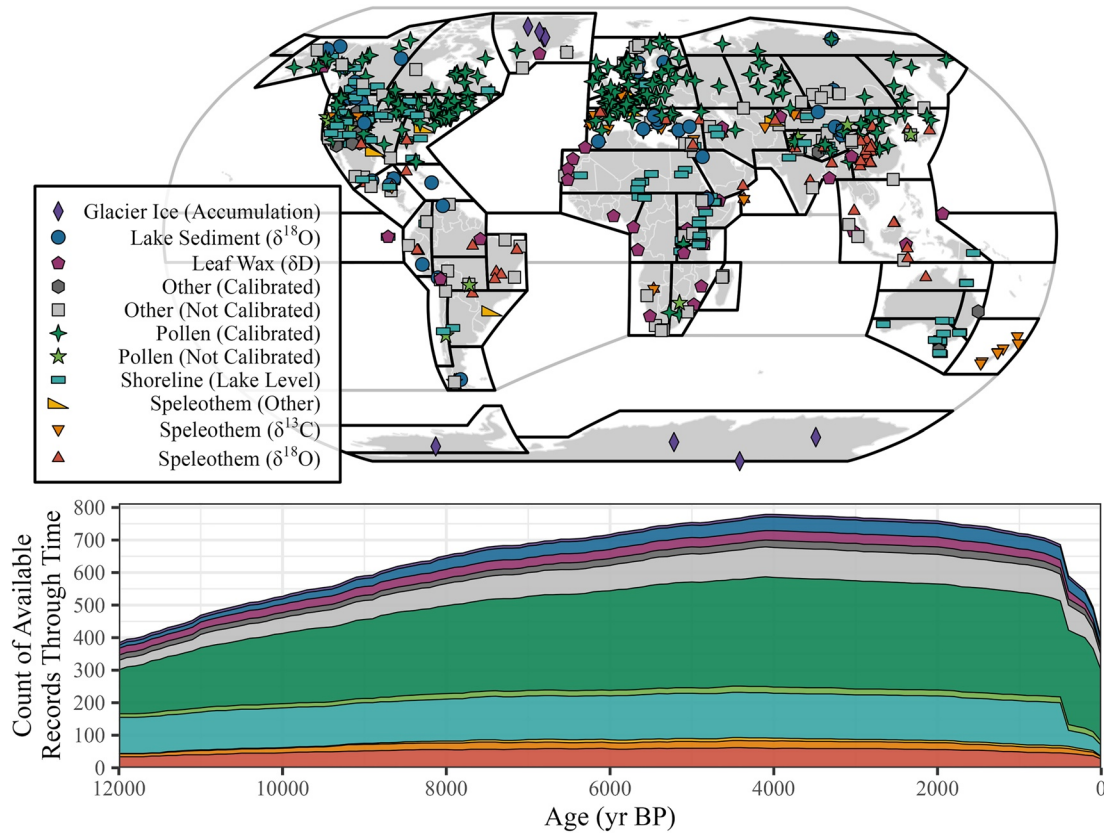


**Figure 1.** Geographic distribution of proxy data (top). Sites symbolized by proxy category (Table 1). IPCC reference regions (Iurbide et al., 2020) shown with solid black lines. Temporal coverage (bottom) shows the number of available records through the Holocene. Values are based on the range between the minimum and maximum age of each record. Colors symbolize proxy categories and match the map legend.

**Table 1**  
*Proxy Record Metadata by Category*

Category <sup>a</sup>	Count (#)	Median duration <sup>b</sup> (years)	Median resolution <sup>c</sup> (years)	Median age control count <sup>d</sup> (#)	Median max age control gap <sup>e</sup> (years)
Glacier Ice (Accumulation)	8	12,000	19	Layer Count	Layer Count
Lake Sediment ( $\delta^{18}\text{O}$ )	43	9,284	31	9	2,070
Leaf Wax ( $\delta\text{D}$ )	31	11,013	150	11	2,345
Pollen (Calibrated)	345	10,820	150	7	2,500
Pollen (Not Calibrated)	19	11,840	87	13	2,395
Shoreline (Lake Level)	139	11,506	1,174	10	2,145
Speleothem ( $\delta^{18}\text{O}$ )	74	8,895	12	15	1,476
Speleothem ( $\delta^{13}\text{C}$ )	28	7,684	26	7	1,631
Speleothem (Other)	9	8,163	34	14	1,184
Other (Calibrated)	23	10,000	106	18	1,326
Other (Not Calibrated)	94	9,542	38	9	2,215
All	813	10,820	109	8	2,370

*Note.* Age control statistics calculated from the 70% of records with a chronology table included in the LiPD file. All values calculated for ages between 0 and 12 ka. <sup>a</sup>Categories are defined based on broad groups of archive, proxy, and measurement types. <sup>b</sup>Duration is the record length calculated as the difference between the maximum and minimum proxy measurement ages. <sup>c</sup>Resolution is calculated as the median difference between proxy measurement ages. <sup>d</sup>The quality of each record's chronology is characterized by the number of age control points. <sup>e</sup>The quality of each record's chronology is characterized by the maximum gap between age control points.

(P-E) ( $n = 305$ ) were included. Records for which the primary sensitivity was identified as changing atmospheric circulation, source water, or seasonality were not included.

Thirty eight percent of the records ( $n = 305$ ) in this compilation are pollen-based precipitation reconstructions from the LegacyClimate 1.0 data set (Herzschuh et al., 2023). The full LegacyClimate data set includes multiple annual precipitation reconstructions for each fossil pollen record using different combinations of statistical methods and training data. We select the weighted-averaging partial-least squares regression (WA-PLS) method based on a precipitation-tailored modern training set as the timeseries most appropriate for our data set. Only those records that passed ( $p < 0.1$ ) the reconstruction significance test listed within the original data set (Herzschuh et al., 2023) and that met the sample resolution and age control criteria of this study were included (12% of the LegacyClimate data set). We preferentially selected the LegacyClimate data over other pollen-based climate reconstructions from the same sites because of their standardized calibration methodology, data format, detailed chronological uncertainty, and significance metrics.

Other major components of the compilation include relative lake level status indicators ( $n = 83$ ) from the global Oxford Lake Status Data Bank (Street-Perrott et al., 1989), North American lake level changes ( $n = 31$ ) from Liefert and Shuman (2020), stable isotope measurements of speleothems ( $n = 94$ ) from SISALv2 (Comas-Bru et al., 2020), and Holocene-length isotope records ( $n = 11$ ) from PAGES iso2k (Konecky et al., 2020). Regional multi-proxy datasets from the Arctic ( $n = 19$ ) (Sundqvist et al., 2014), Northern Hemisphere midlatitudes ( $n = 9$ ) (Routson et al., 2019), and western North America ( $n = 19$ ) (Routson et al., 2021) were included. Additional records ( $n = 242$ ) from local compilations and individual sites were obtained from the primary literature.

Data not already available in Linked Paleo Data (LiPD) format were converted to LiPD, which facilitates data analysis using standardized, machine-readable metadata (McKay & Emile-Geay, 2016). We followed the data and metadata conventions used in previously published LiPD-based compilations (Kaufman, McKay, Routson, Erb, Davis, et al., 2020; Konecky et al., 2020; Routson et al., 2019), and important metadata labels are defined in Table S1 in Supporting Information S1. A full list of proxy data sites, including their metadata and source, is also provided in Table S1 in Supporting Information S1.

Criteria for inclusion in the compilation were consistent with Temp12k (Kaufman, McKay, Routson, Erb, Davis, et al., 2020). Specifically: (a) the age range covers a minimum of 4 ka between 0 and 12 ka, (b) the median spacing between measurements spans fewer than 400 years during the record length within the past 12 ka, and (c) the record's chronology includes a control point at least every 3 ka or a relatively even spacing ( $<4$  ka) of at least five control points during the Holocene (Table 1). Exceptions to the criteria are stated in the metadata for each LiPD file. For records with ages published in radiocarbon years, ages were converted to calendar years BP using geoChronR (McKay et al., 2021) and by OxCal (Martin et al., 2021) using the IntCal20 radiocarbon age calibration curve (Reimer et al., 2020).

The lake level data from the Oxford Lake Status Data Bank (Street-Perrott et al., 1989) did not meet all of the criteria because they have coarse temporal resolution ( $>1$  ka between data points) and are ordinal rather than numerical (i.e., categorized as “low”, “medium”, and “high” estimates of lake level). Nonetheless, their global spatial coverage and full-Holocene length provides valuable insight for data-sparse regions such as North Africa and Australia. Furthermore, these data provide a direct physical record of hydrologic change for which to compare less direct proxy types such as those relying on isotopic interpretations or pollen calibrations (Lézine et al., 2011). Where available, these lake level records were replaced by newer, higher resolution data by Liefert and Shuman (2020) for North America and by additional individual publications for other regions.

For sites where a single proxy type is used to reconstruct hydroclimate for both an annual average and for different seasons (e.g., summer and annual precipitation calculated from the same pollen assemblages), we used the average annual values, but the seasonal reconstructions were also retained in the data set and are labeled as “Winter+” or “Summer+” in the seasonality metadata. Otherwise, all hydroclimate-sensitive timeseries from each site are included. Although this may overrepresent sites with multiple records, few sites are presented by more than three proxy types, and sites with multiple proxy types provide a diverse sample of climate variability based on different proxy system processes.

## 2.2. Regional Hydroclimate Composites

The spatial heterogeneity and complex dynamical forcing of hydroclimate variability necessitates the clustering of proxy sites geographically. We adopt the IPCC AR6 climate reference regions (Iturbide et al., 2020), each

of which represents a somewhat homogenous climatology independent from the proxy data set. Although these spatial boundaries are based on the modern climatology and may not perfectly represent Holocene climate shifts, they provide a simple framework for comparing the regional characteristics of proxy and model data. For regions with at least six proxy records, a composite was calculated to represent regionally averaged Holocene hydroclimate changes. Identifying the minimum number of records necessary to represent a region is challenging because varying proxy geographies, resolutions, and interpretations influence the representativeness of any subset of records. To evaluate the suitability of the six-record threshold, we compared two climate-model-simulated timeseries for each region: (a) the simulated precipitation based on the mean of all grid cells within a region, and (b) the mean of the grid cell nearest to each proxy location (effectively, the mean of a pseudo-proxy network). The results (Figure S1 and Table S3 in Supporting Information S1) indicate that although more records generally improve the estimation of a regional average, the results are highly variable and model dependent. Further analysis to assess proxy agreement within each region is described in Section 2.4. The six-record minimum avoids the most significant impacts of small sample sizes while maximizing the number of regions included in this study.

We make two exceptions to the six-record minimum criterion, both located in the Southern Hemisphere, to provide a more global view of Holocene hydroclimate. First, southern South America, with only four records of varying proxy types, is included because it provides potential insight into midlatitude variability. Second, East Antarctica only has three ice accumulation records, but each has high measurement resolution and strong age control.

Fewer than half of the records (45%) are calibrated from proxy units to precipitation or P-E values. Therefore, rather than using primary units (e.g., mm/year), proxy data within each region were standardized by iteratively ( $n = 500$ ) matching the mean and standard deviation of each record over a randomly selected interval using the `compositeR` package. This standardization technique adjusts the mean and variance of each record to minimize differences during the defined window and applies this conversion to all values over the Holocene. The procedure is similar to the dynamic calibrated composite (DCC) method used to reconstruct zonal-mean temperatures from the Temp12k data set (Kaufman, McKay, Routson, Erb, Dätwyler, et al., 2020). Before compositing, records were interpolated using a nearest neighbor approach, and binned into 100-year segments to approximate the median resolution of the data set (109 years). We use a relatively narrow 3,500-year standardization window to limit spurious comparisons between records over periods with different boundary conditions. Randomly shifting the window allows all records to contribute to the resulting composite without removing those that do not overlap with a predefined search range. The iterative approach produces a 500-member ensemble with each timeseries computed as the mean of the proxy records relative to a specified standardization window.

### 2.3. Climate Model Simulations

Results obtained from analysis of the proxy records were compared with transient simulations from two independent general circulation models (GCMs). (a) The TraCE-21k simulation (TRANSient Climate Evolution over the last 21,000 years) (He, 2011), which was run using NCAR's CCSM3 climate model (Collins et al., 2006), is often used in studies evaluating proxy-model agreement (e.g., Lu et al., 2019; Ning et al., 2019). (b) We also include the HadCM3 transient deglaciation (deglh) simulation of the UK Met Office's HadCM3 (Hadley Centre Coupled Model, version 3) climate model, which follows PMIP4 protocol including orbital configuration and greenhouse gas concentrations (Ivanovic et al., 2016). Henceforth, these simulations will be referred to as "TraCE" and "HadCM."

However, computational requirements for coupled transient ocean-atmosphere simulations are high and data for the entire Holocene are limited to these two models. Therefore, we also analyze 12 CMIP6-PMIP4 time slice simulations (Table S2 in Supporting Information S1) for the mid-Holocene (6 ka) to provide a more diverse ensemble of plausible climate states based on the range of model-specific parameters and feedback processes. Time-slice values from TraCE and HadCM are calculated as the difference in millennial averages centered on 12, 6, and 0.5 ka. Model comparisons were performed after spatial regridding (Zhuang et al., 2020).

Regional timeseries were also calculated for the two transient model simulations based on 100 years means of annual precipitation. A land mask was applied to exclude values over the ocean. Although the proxy data include marine records, such as isotopes in plant material (e.g., Tierney & deMenocal, 2013) and elemental composition of sediments (e.g., Jaeschke et al., 2007), these proxies overwhelmingly reflect terrestrial processes. We focus

on annual precipitation because the majority (62%) of proxy records are interpreted to reflect this variable, and the simulated precipitation change dominates P-E variability for most locations over these timescales. Overall differences between P and P-E simulations are relatively small, and all figures shown in the main text of this paper display annual precipitation values. Because many of the proxy data represent qualitative changes, we focus on relative changes in simulated precipitation amount rather than the magnitude of anomalies.

#### 2.4. Mid-Holocene Anomalies

An ensemble of 12 CMIP6 models were used to simulate mid-Holocene climate relative to their preindustrial control runs (Table S2 in Supporting Information S1). As with the transient simulation timeseries, regional anomalies were calculated using the mean anomaly for all grid cells covering land. These data were compared to the transient simulations and proxy data by using the mean value within a 1,000-year time slice centered on 6 ka and 0.5 ka.

In addition to the magnitude of change, we also compared the sign of the mid-Holocene change relative to the preindustrial and last millennium values to gauge consensus within proxy and model data. For proxy data, the percentage of proxies with positive versus negative mid-Holocene anomalies were calculated relative to the total number of records with data within each time slice. For the 14 model simulations, data regridded to a common spatial resolution were similarly compared to calculate the percent of simulations with a positive anomaly for each grid cell.

#### 2.5. Temperature

Regional reconstructions and mid-Holocene anomalies were also calculated for temperature proxies and model simulations. Proxy data are from the Temp12k compilation (Kaufman, McKay, Routson, Erb, Davis, et al., 2020). Based on these results, and to further understand the relationship between temperature and hydroclimate, we correlated simulated mean annual precipitation with surface temperature at the grid-cell scale. We also correlated the proxy ensemble composites of hydroclimate and temperature for regions with sufficient data.

### 3. Results

#### 3.1. Proxy Composites

Composite timeseries reveal large scale patterns in regional hydroclimate across Earth's land regions during the Holocene (Figure 2). Many tropical regions throughout the Northern Hemisphere show a coherent “wet-to-dry” or “dry-wet-dry” signal tracking changes in summertime insolation at low latitudes (Figure 3). This summer sensitivity reflects a combination of the dominance of monsoon circulation on annual precipitation changes and the inclusion of proxies with summer sensitivities within most of the regional composites. In the Southern Hemisphere tropics, this temporal pattern is reversed, with dry mid-Holocene conditions reflective of weaker southern African and South American Monsoons. For both hemispheres, a trend toward modern values begins approximately 6 ka. This reinforces the importance of meridional shifts in the position of the ITCZ in driving global monsoon circulation (Cheng et al., 2012) in parallel with summer insolation throughout the Holocene.

However, not all tropical regions respond similarly to shifting monsoon circulation, and those regions outside of the “core” monsoon domain may reflect more local atmospheric dynamics (Mollier-Vogel et al., 2013) or ocean circulation response (Asmerom et al., 2007). For example, in equatorial southeast Asia, early Holocene variability is forced by sea level rise, which enhanced atmospheric convection as the Sahul and Sunda shelves flooded (Krause et al., 2019).

Outside of the tropics (Figures 2m–2a, and 2b), a gradual but steady trend toward increased moisture throughout the Holocene in North America, central Europe, and Siberia suggests an important role for the strengthening westerly-jet system, consistent with a steepening of the latitudinal thermal gradient. This pattern is especially constant across the three United States regions for which proxy data within the 40–50° latitudinal band are the major contributor to this signal. Further south, greater disagreement is influenced by more variable climate dynamics. In both tropical and extratropical regions, mean states during the early and mid-Holocene differ substantially from the composite values during the common era.

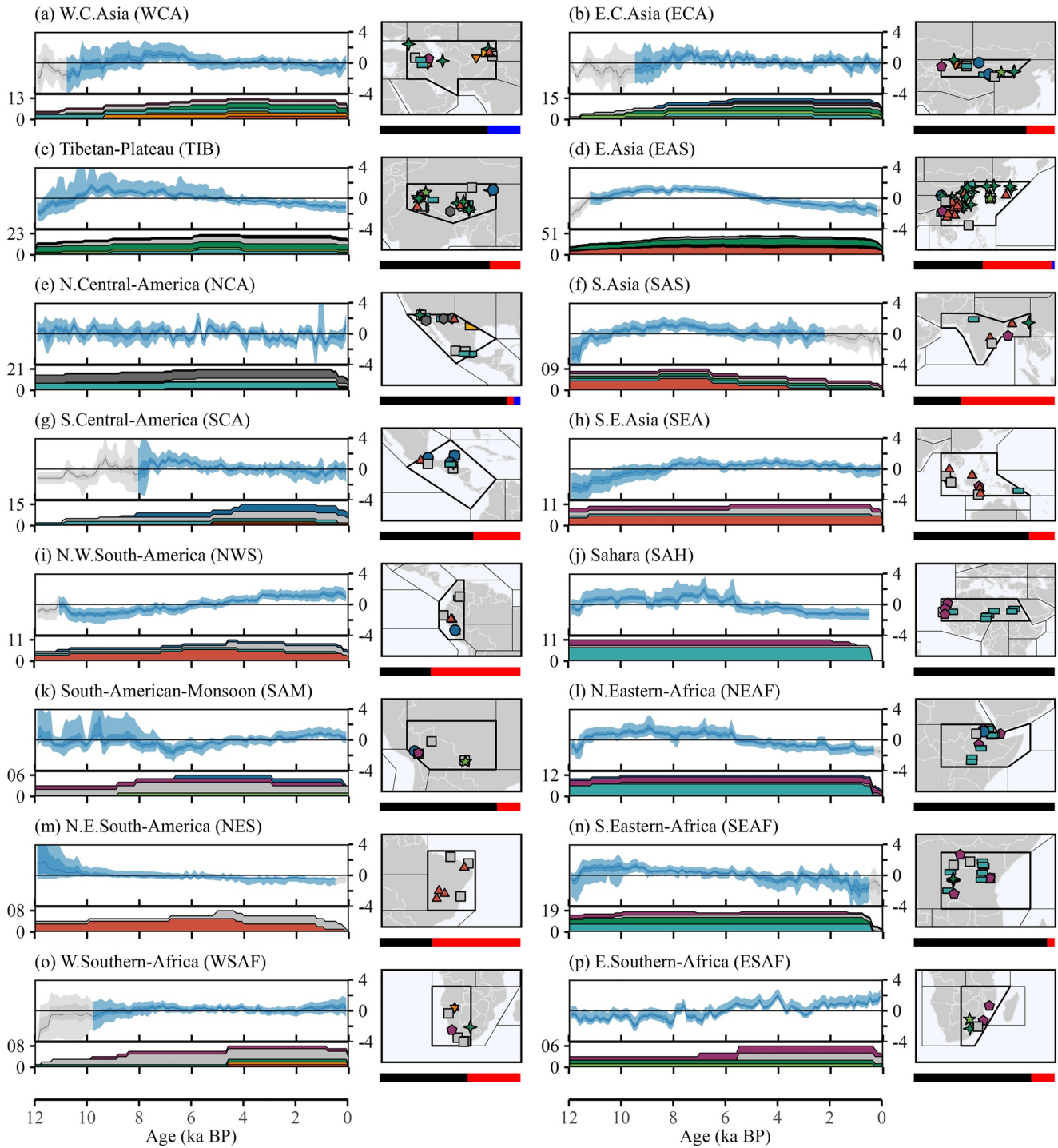


**Figure 2.** Proxy composite timeseries. Y-axes (right side) show z-score anomalies. Gray shading signifies portions of the timeseries when fewer than 50% of proxy records contribute to the timeseries. The dark and light blue and gray shaded envelopes indicate the 50% and 95% quantiles of the ensemble range, respectively. Colors and symbols for the maps and temporal coverage plots match Figure 1. Bars under the maps represent the proportion of annual (black), summer (red), and winter (blue) records. The regions are arranged according to geographic proximity and divided between tropical (a–p) and extratropical (q–af) locations. Region domains and names are according to Iturbide et al. (2021).

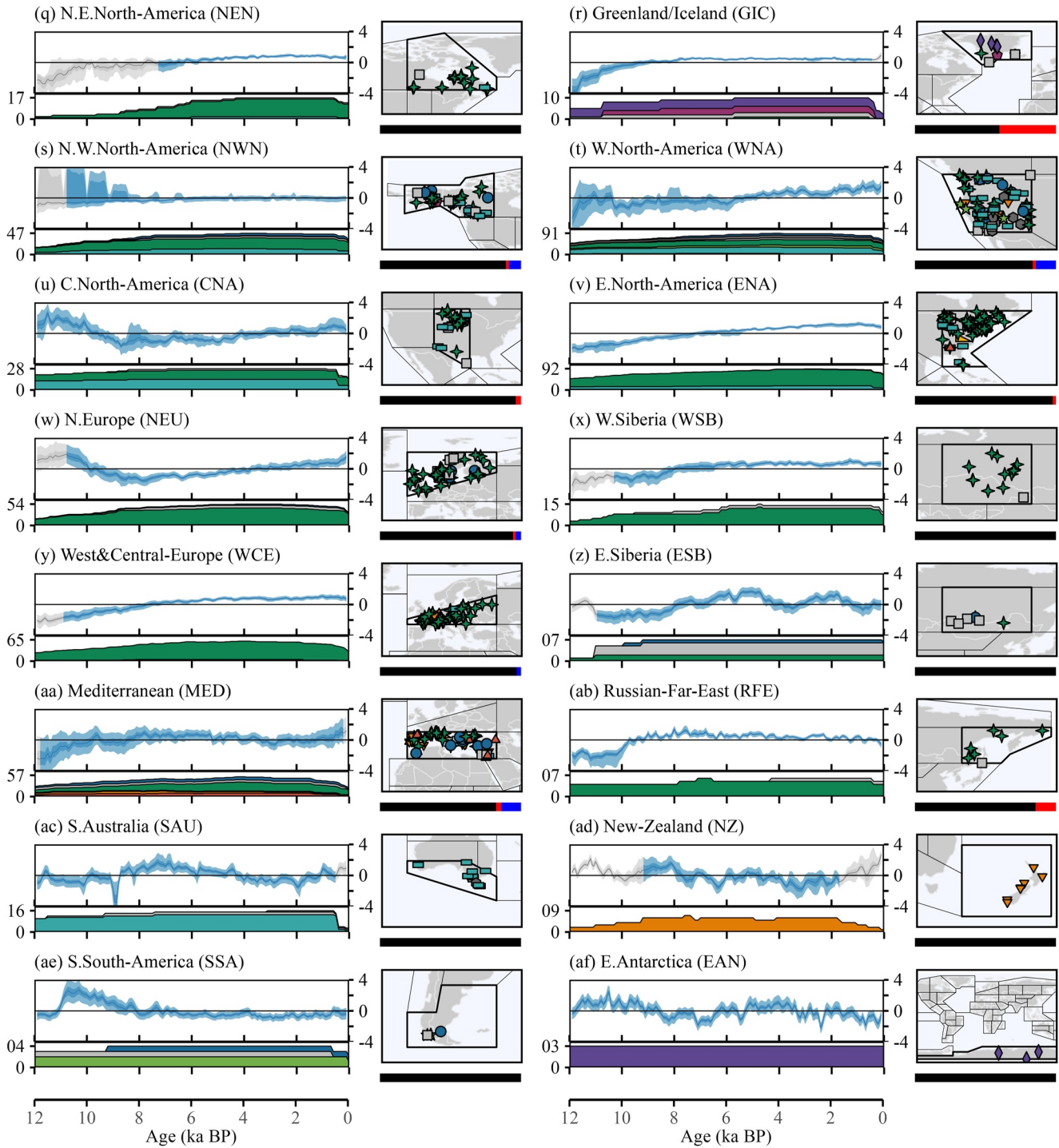
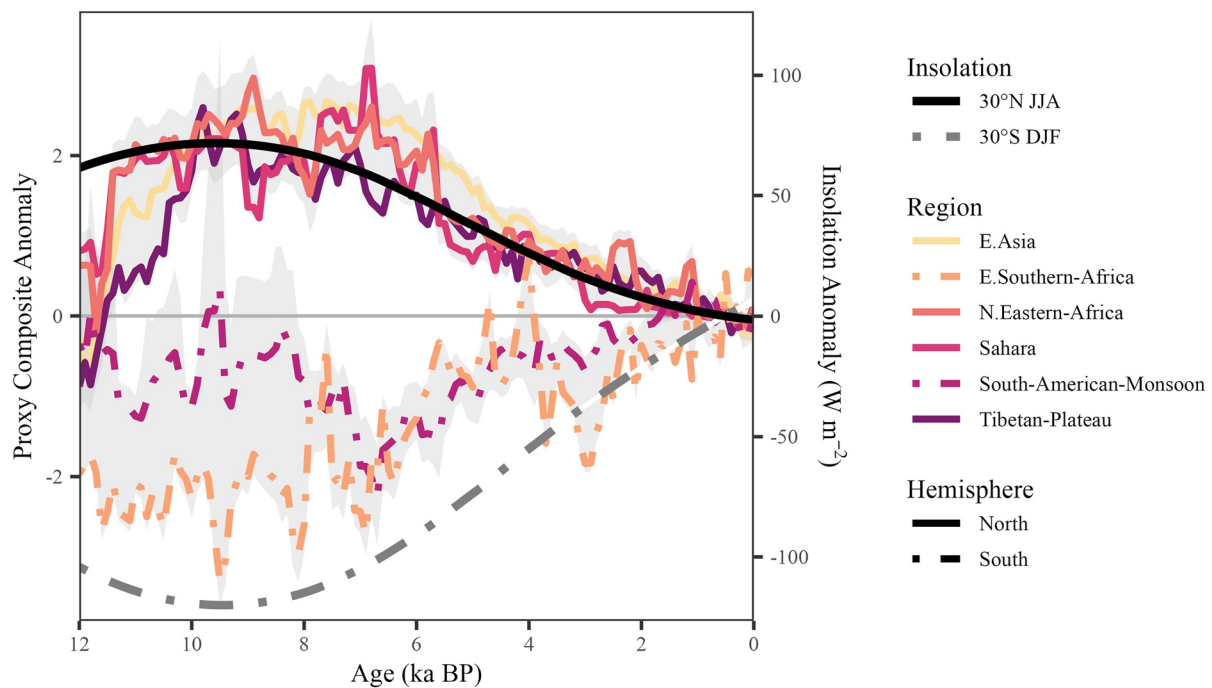


Figure 2. (Continued)

In the Southern Hemisphere, a smaller proportion of the area is covered by land and proxy records are scarcer. However, southern South America, southern Australia, and New Zealand provide information proximal to the southern westerly winds. Proxy records from these regions mostly indicate a drying trend between 8 and 2 ka followed by wetting until present.



**Figure 3.** Proxy record composites from monsoon regions. Summer insolation anomalies at 30° north and south are plotted for comparison (Berger & Loutre, 1991). Composites are median ensemble members plotted relative to their last millennium average (0–1 ka). Gray shading shows the 10%–90% quantiles of the aggregated ensembles for each hemisphere.

### 3.2. CMIP6 Simulations

Many of the major spatial patterns of mid-Holocene hydroclimate anomalies are consistent in both the proxy composites and the CMIP6 ensemble mean (Figure 4), particularly where the magnitude of the change is large. Increased precipitation over portions of India, East Asia, and North Africa during summer (JJA) months (Figure 4b) mark the strengthened monsoon system during the early and mid-Holocene, whereas dry summer (DJF) conditions are simulated in the South American and south African Monsoon regions (Figure 4c).

In the midlatitudes, the magnitude of change is smaller, but dry mid-Holocene anomalies are widespread across large portions of the northern Eurasian continent, especially in summer months when increased insolation forced a weakened hemispheric LTG (Zhou et al., 2020). More complex patterns are observed for North America, with increased summer precipitation across the East Coast and the U.S. Southwest during the mid-Holocene. This contrasts with dryer conditions in the central continent.

### 3.3. Transient Simulations

Annual precipitation anomalies were also calculated for both transient simulations (Figure 5). Time slice differences were chosen to better compare the CMIP6 and transient results and because the wettest and driest centuries tend to occur at either the beginning or end of the Holocene (Figure S2 in Supporting Information S1). Major patterns of 6–0.5 ka anomalies from the two transient simulations (Figures 5b and 5d) resemble each other and those of the CMIP6 time slice simulations. The transient simulations show regional shifts between wet and dry regional anomalies that are larger than the CMIP6 average, likely because of the smoothing inherent in the ensemble mean.

The 12 ka time slice represents conditions that are considerably different from the mid-Holocene, and is included for a more complete analysis of Holocene hydroclimate. During the first half of the Holocene (12–6 ka), simulated precipitation anomalies in the tropics tend to show the opposite trend compared with the late Holocene (6–0.5 ka). For example, increased precipitation at 6 ka relative to 12 ka in portions of North Africa, Asia, and Central America and decreased precipitation in South America, southern Africa, and Northern Australia are reversed during 6 ka relative to the last millennium. Changes in the extratropics are typically more consistent between the two time periods. For example, dry precipitation anomalies in northern Eurasia and Antarctica indicate a continued wetting trend through the Holocene.

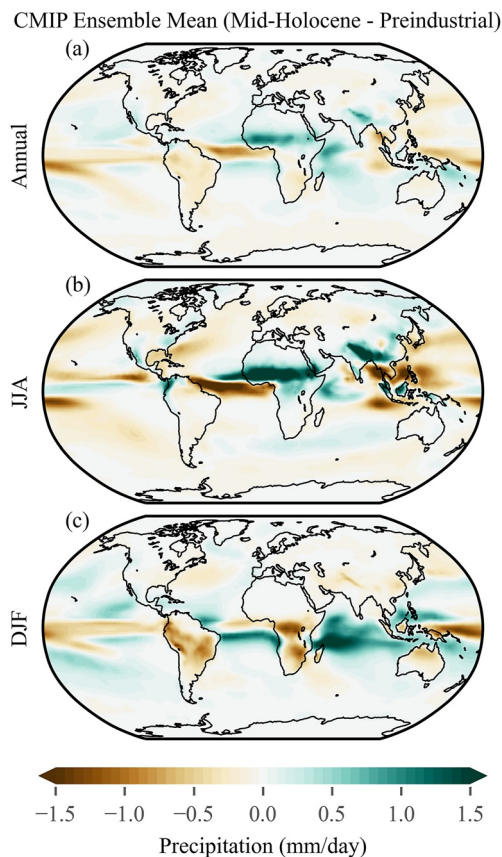


**Figure 4.** Mid-Holocene precipitation anomalies for the CMIP6 ensemble mean. Green colors signify greater precipitation during the mid-Holocene relative to preindustrial and brown colors indicate drier conditions. Values represent the mean during (a) annual, (b) boreal summer, and (c) boreal winter.

The pattern of P-E anomalies (Figure S3 in Supporting Information S1) generally matches these results. One notable exception appears near remnant ice sheets such as in central Canada and Fennoscandia where lower precipitation at 12 ka relative to 6 ka contrasts with high P-E anomalies. This apparent discrepancy likely indicates significant increases in evaporation after the ice sheets diminished.

## 4. Discussion

### 4.1. Proxy-Model Comparisons

The proxy composite timeseries represent a relative scale of wetter or drier. Therefore, comparisons between proxy and model results focus on long-term trends, spatial patterns, and timing of hydroclimate change throughout the Holocene. Globally, the proxy composite and model simulation results show substantial moisture anomalies during the early and mid-Holocene relative to that of the last millennium, and the direction of these anomalies vary by region. We organize this discussion to highlight different atmospheric circulation patterns within tropical, midlatitude, and high-latitude regions.

#### 4.1.1. Tropics

Overall agreement between proxy and simulated results is particularly evident in southern Asia and North Africa where numerous regional timeseries reconstruct early and mid-Holocene wet periods (Figure 6). In the Southern Hemisphere, an opposite (dry-to-wet) pattern is shown in the proxy composite and CMIP6 simulations in the South American Monsoon, N.W. South America, and E. southern Africa regions. The transient simulations, particularly TraCE, are mixed in their agreement with the proxy records, but differences might reflect the incomplete coverage of proxy records within some regions. This is evident for N.W. South America where wetter conditions in the north counterbalance the dry anomaly observed in the south (Figure 4). Proxy composites for tropical regions outside of the major monsoon systems, such as northern Central America and N.E. South America, show minimal trends throughout the Holocene that agree with simulated precipitation.

#### 4.1.2. Midlatitudes

Throughout North America and central Asia, many of the proxy composites show a coherent long-term wetting trend. Although the magnitude of change may have been less than tropical regions (Figure 4), small but compounding changes in hydroclimate can have significant environmental impacts (Shuman & Marsicek, 2016). Previous research has noted this pattern and hypothesized that the trend was a response to a weakened LTG and westerly circulation (Routson et al., 2019; Zhang et al., 2017). The proxy compilation presented here supports these results and improves the spatial distribution of proxy data with notable additions throughout Eurasia. Furthermore, the regional composites provide additional spatial resolution for this wetting trend.

Models generally agree with the proxies for Eurasia where an increasing precipitation trend is simulated for northern/central Europe and the Siberian regions, consistent with insolation-driven strengthening of the westerly jet stream (Zhang et al., 2016; Zhou et al., 2020). However, results from eastern and western North America regions show notable disagreement between proxy composite (wetting) and transient model (drying) trends. Although models simulate higher annual precipitation in the past, winters may have been dryer during the mid-Holocene (Figure 4). In North America, summer and winter trends are similar, but the number of these records is minimal (Figure S4 in Supporting Information S1). Pollen and lake level records, the main source of the wetting trend, are interpreted to represent annual conditions, but a possible winter bias could explain a portion of the proxy-model disagreement (Commerford et al., 2018). For some regions, a subset of the CMIP6 ensemble provides model solutions consistent with the proxy data at 6 ka (Figure 6). For example, in western North America, a subset of models simulating less westerly moisture transport better agree with the proxies (Hermann et al., 2018).

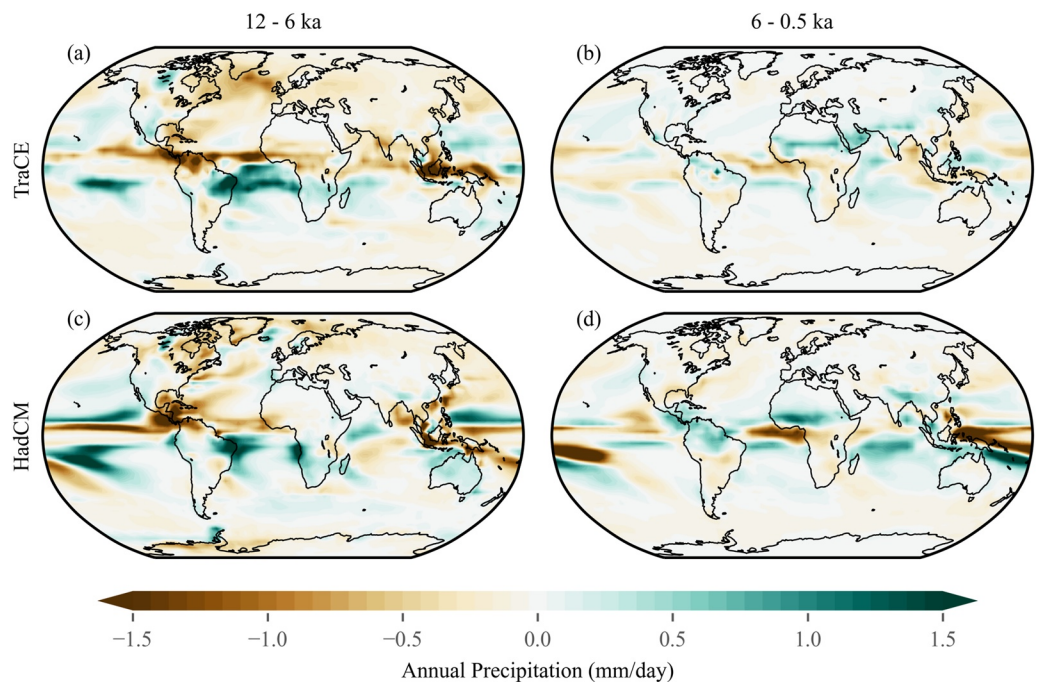


**Figure 5.** Annual precipitation anomalies for two time slices from two transient simulations. Maps show the mean difference between 1,000-year bins centered on (a,c) 12 and 6 ka (i.e.,  $12 \pm 0.5$  ka minus  $6 \pm 0.5$  ka), and (b,d) 6 and 0.5 ka. Green and brown colors indicate wetter and drier conditions, respectively, during the earlier period. The 6–0.5 ka values (right column) are analogous to the CMIP6 values shown in Figure 4a. The same figure, but showing P-E anomalies, is in Figure S3 in Supporting Information S1 for comparison.

In the Southern Hemisphere midlatitudes—southern South America, southern Australia, and New Zealand—proxy composites show a drying trend between 8 and 2 ka (Figure 2). Original publications of the proxy data support the hypothesis that diminishing westerly circulation through the Holocene, either from weaker winds or a poleward shift of the circulation belt, resulted in reduced moisture delivery from this source and a shift to more equatorial forcing on orbital timescales (Bernal et al., 2016; Gomez et al., 2013; Rees et al., 2015). This is consistent with a decreasing LTG estimated from proxy records of sea surface temperatures (Voigt et al., 2015), and in opposition to the Northern Hemisphere insolation trend. However, for each region, conclusions are complicated by the impacts of seasonality, meridional circulation shifts, and local climate dynamics as well as the sparse geographic distribution of the available proxy data (Chase et al., 2015; Lamy et al., 2010).

#### 4.1.3. High Latitudes

The Greenland/Iceland and East Antarctica regions are the two highest latitude regions with enough proxy records to calculate a composite timeseries. In Greenland, a strong wetting trend during the early Holocene is followed by climate stability after 6 ka (Figure 6). This coincides with well-documented early Holocene Arctic warming followed by gradual cooling (Kaufman, McKay, Routson, Erb, Dätwyler, et al., 2020). Further connecting precipitation and temperature, wet summer anomalies occur during the mid-Holocene (Figure 4) when proxy and model results agree about summer warming. This hydroclimatic trend appears representative as simulated precipitation from other Arctic regions also indicates early wetting followed by stable values after 6 ka (Figure 5).

In East Antarctica, the hydroclimate composite, which is based on ice accumulation records, provides no evidence for any long-term trend throughout the Holocene. Temperature reconstructions from this region also indicate minimal variability during this time (Kaufman, McKay, Routson, Erb, Dätwyler, et al., 2020). In contrast, models simulate both warming and wetting trends, particularly for the early Holocene, across much of the continent. The general lack of Holocene hydroclimate proxy records at southern high latitudes limits our interpretation; however, these results are consistent with the observed and hypothesized correlation between temperature and precipitation in polar regions (Bintanja & Selten, 2014; McCrystall et al., 2021).

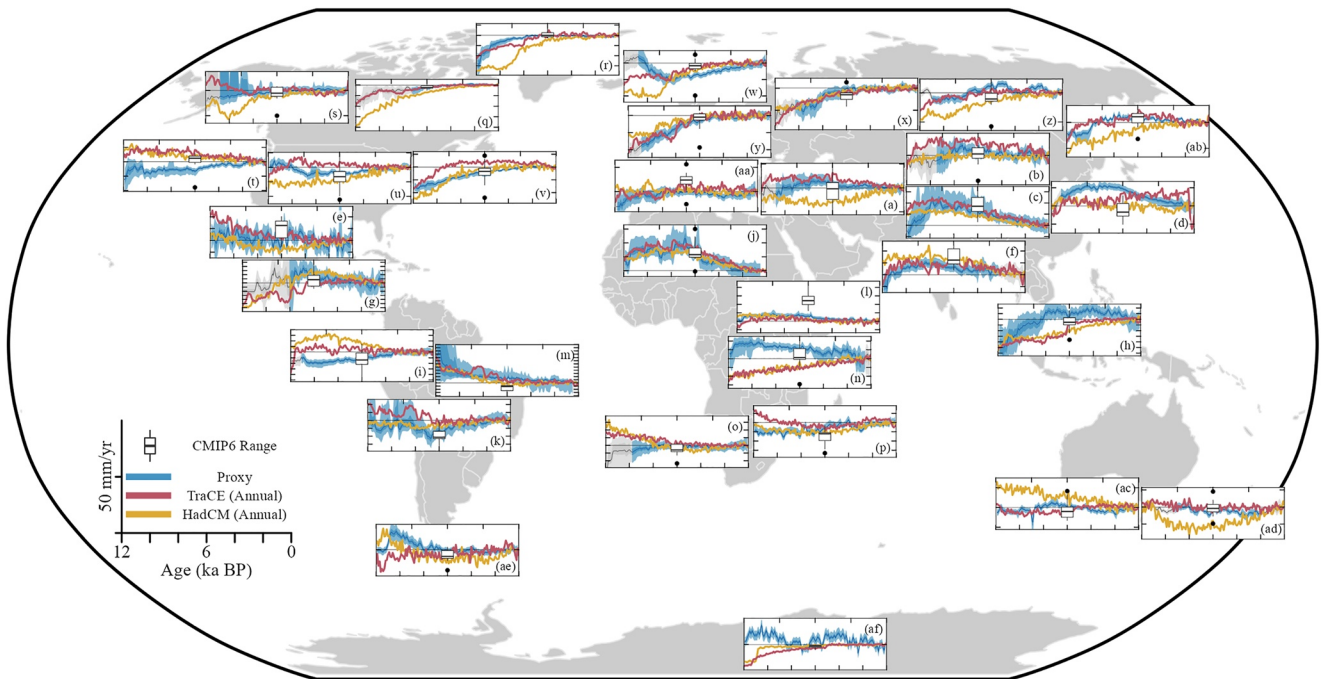


**Figure 6.** Comparison between proxy composite and simulated regional annual precipitation timeseries. TraCE (red) and HadCM (yellow) timeseries of mean annual precipitation (mm/year). Boxplot at 6 ka is based on the 12 model CMIP6 ensemble. Model timeseries are calculated as the latitude-weighted mean of all grid cells over land within each region. The variance of each proxy (blue) ensemble is scaled to match the average centennial-scale variance of the two transient timeseries. The y axes for each plot are adjusted to fit the full range of variability within that region over the Holocene. In all plots, each y-axis tick indicates a change of 50 mm/year. All data are shown as the difference relative to the last millennium average, which is shown by the black horizontal line, and positive values (up) indicate wetter conditions. Letters in the corner of each plot indicate the region as marked in Figure 2. Similar to Figure S5 in Supporting Information S1, which shows temperature.

#### 4.2. Temperature Correlations With Hydroclimate

These datasets and simulations allow us to systematically explore the relationship between precipitation and temperature. Here we calculate centennial-scale correlation coefficients between the two variables as simulated by both transient simulations and represented in regional proxy composites calculated from Temp12k and our hydroclimate data set (Figure 7).

Because models indicate widespread warming throughout the Holocene, positive correlation coefficients are typically associated with regions experiencing wetting trends. The primary exception is the Arctic where positive correlations result from simulated cooling and drying during the late Holocene. The high latitudes include the highest zonal correlation coefficients, which signifies the temperature dependence of precipitation for these regions in response to albedo and water vapor feedbacks (Bintanja & Selten, 2014; McCrystall et al., 2021). In Northern Hemisphere monsoon regions, simulated temperature and precipitation are inversely correlated where wet conditions are associated with cooler temperatures in the early Holocene. In the midlatitudes, the relationship between temperature and precipitation is less well-defined. Complicated correlation patterns in the midlatitudes contrasted with a positive relationship in polar regions were also reported by Herzschuh et al. (2022) using the TraCE simulation and pollen records.

Correlations between temperature and precipitation in proxy records are limited to the 23 regions that include sufficient ( $n > 6$ ) data to create composite timeseries. In the tropics, the positive relation between the two climate variables in the proxy data contrasts with the negative correlation in the simulations. The insolation-driven peak in Northern Hemisphere monsoon circulation and regional precipitation coincides with warmer temperatures in the proxy data. As a result, correlations are positive in Asia and North Africa. Model simulations, however, do not simulate warm surface air temperature in those regions during the mid-Holocene, resulting in negative correlations between temperature and precipitation simulated by models. This represents a major disagreement between model simulations and proxy data, and the competing roles of insolation-forced radiative warming versus cooling driven by increased cloudiness and evaporation in monsoon regions.

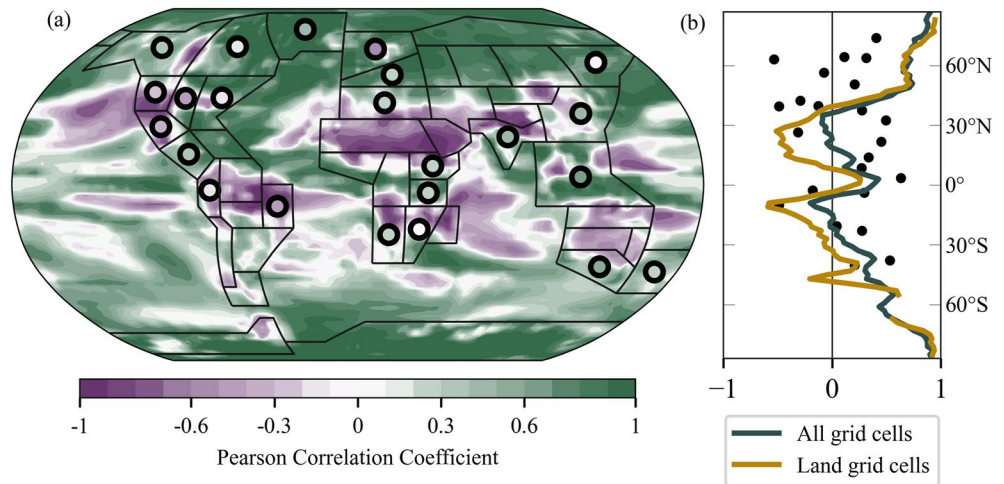


**Figure 7.** Correlation between precipitation and temperature in Holocene climate simulations and proxy records. (a) Map colors show the mean correlation between the two climate variables from the HadCM and TraCE simulations. Circle colors indicate the correlation from the proxy composites. More saturated colors represent stronger correlations. (b) Zonal average of correlations from simulations (lines) and from regional proxy composites (dots) shown in panel (a). All correlations calculated using data binned to 100 years.

### 4.3. Sign of 6 Ka Anomalies and Evaluating Proxy–Model Agreement

To simplify the proxy–model comparison, we focus on just the sign of mid-Holocene precipitation anomalies to evaluate where the two data types agree whether climate was wetter or drier relative to modern (Figure 8a). Because the analysis is based on the direction of change, the results are unaffected by the normalization of measurement values. Thus, the results can provide insight into where different proxy types indicate a robust consensus, or lack thereof. Although this metric is basic, proxy records and model simulations fail to reproduce the same sign for temperature (Figure 8b).

For hydroclimate, results indicate that regions where the magnitude of precipitation change is large, typically due to changing monsoon intensity, also show the strongest agreement among the sign of proxy records and between

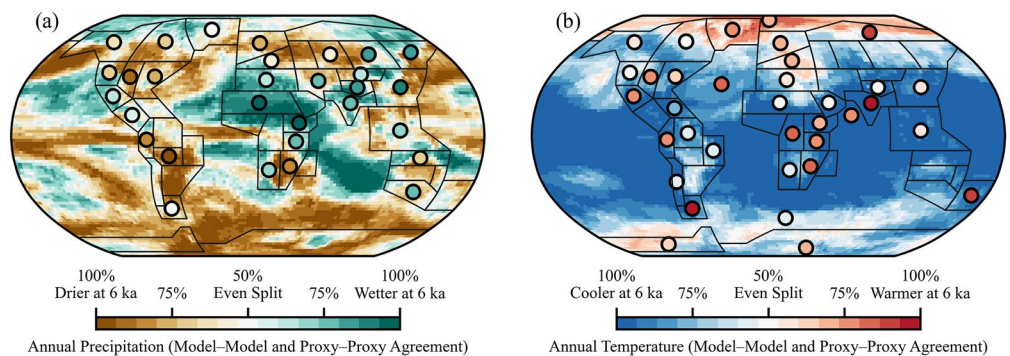


**Figure 8.** Agreement of the sign of mid-Holocene annual (a) precipitation and (b) surface air temperature anomalies relative to preindustrial. Model-to-model agreement is indicated by the color of the base map, and proxy-to-proxy agreement is indicated by colors of circles within regions, where more saturated colors on either end of the scale represent stronger agreement. Proxy–model agreement is indicated by the similarity between the map and circle colors. Models include TraCE, HadCM, and the 12 CMIP6 simulations, all regridded to a common spatial resolution (2.66° longitude by 2° latitude). Each color step from left to right on the color bar represents one additional model among the 14 with a positive (wetter or warmer) mid-Holocene anomaly. For the two transient models, signs represent the difference in mean values between 6.5–5.5 ka and 1–0 ka. The agreement among proxy records (colored circle within each region) is represented as the proportion of available proxy records with positive anomalies during the mid-Holocene (6.5–5.5 ka average) relative to the last millennium (1–0 ka average). Available records are defined as those with at least one data point within both the mid-Holocene and last millennium age ranges. Circles are only shown for regions with at least four available proxy records.

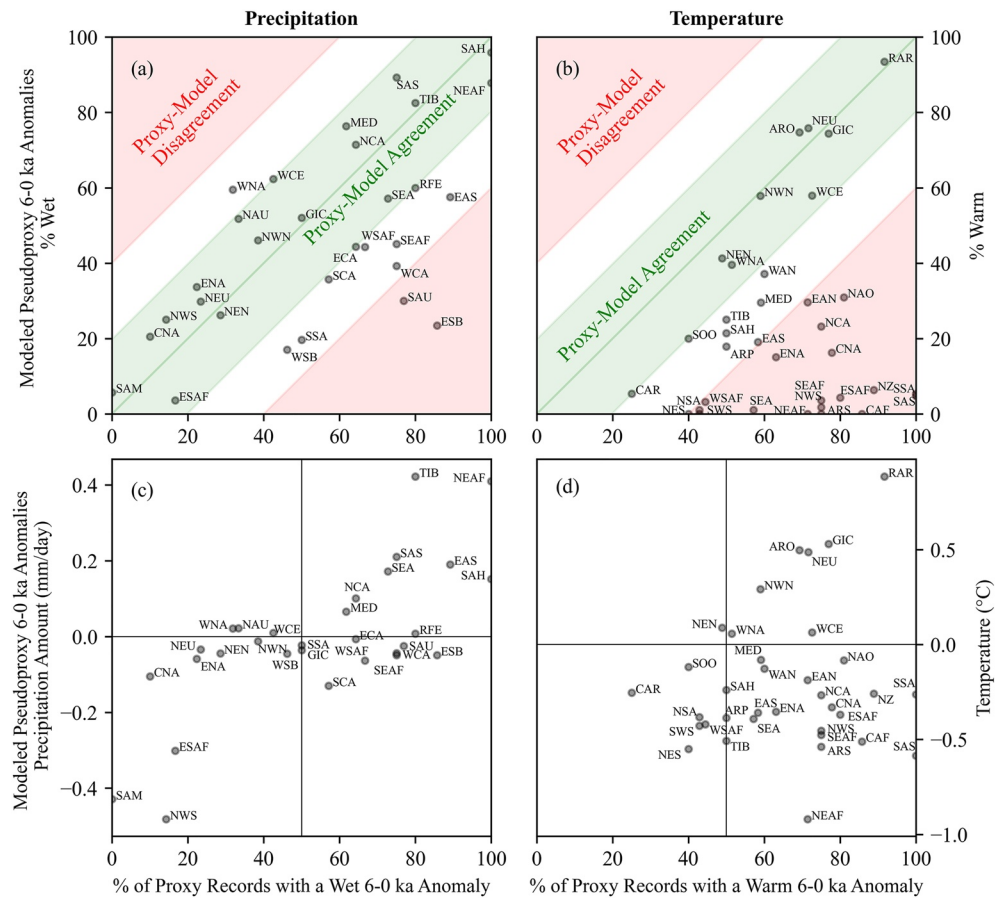


**Figure 9.** Scatterplot showing the extent of proxy–model agreement from Figure 8. Percent of proxy records within each region with a (a) wet or (b) warm mid-Holocene anomaly, each plotted against the percent of pseudoproxies with a corresponding anomaly. Perfect agreement is represented by a 1:1 line. Pseudoproxies represent model values calculated using the geographic locations and seasonality metadata of the proxy records. The regional percent is calculated as the mean of the percent of positive anomalies for each proxy site relative to the 14-model ensemble. Panels (c, d) same as (a) and (b), but showing the mean magnitude of the simulated anomaly for each proxy site. Regional abbreviations are in Figure S6 in Supporting Information S1 and Figure 2.

proxy and model data (Figure 9). Because proxy records integrate complex relationships between climate variables and their archived responses, a higher signal-to-noise ratio in regions with larger climate anomalies may be needed to accurately represent the direction of change. Additional factors such as the variety of proxy types within a region may also influence agreement among proxy data. Among the model ensemble, agreement is more widespread, and consistent signs of mid-Holocene anomalies are observed for some regions despite relatively small magnitudes of change. For example, in portions of northern Eurasia and the Southern Ocean, all models simulate the same direction of change (Figure 8a) for these minor trends (Figure 4a).

However, in some regions, the uncertainty among the proxy data is also reproduced by the model ensemble. For several regions with poor proxy-to-proxy agreement, such as western central Asia and southern Central America, proxy disagreement is consistent with models, which are uncertain about the sign of change (Figure 8a). For some regions, such as central Europe and N.W. North America, a mixed climate signal might be explained by an intra-regional dipole. Nonetheless, for some midlatitude regions, a clear consensus among models is either not matched by the proxy records or is in the opposite direction. This is most apparent in western North America where most models simulate wet conditions while most proxy records indicate dryer conditions and in Eastern Siberia where dry models oppose wet proxy values (Figure 8a).

For evaluating global proxy–model agreement, we compare two values (a) the number of proxy records which indicate a positive (wet) anomaly and (b) the same metric based on a pseudoproxy network calculated from

the model simulations controlling for the geographic bias and seasonality of the proxy data. We then count the number of regions for which the two percentages are within 20% of each other or differ by more than 40%. Based on these thresholds, 19 of the 30 (63%) regions are in agreement compared with only two in disagreement (Figure 9a).

For temperature, proxy records and model simulations both show warming during the first half of the Holocene (Figure S5 in Supporting Information S1), but results differ regarding mid-Holocene temperature anomalies. Higher temperature at 6 ka relative to the last millennium is widespread for the proxy data, with many regions (19 of 35) showing proxy–proxy agreement for warmer temperatures and only one showing agreement for cooler temperatures (Figure 9b). The remaining 15 regions show mixed signals (40%–60% agreement). By contrast, models, even when controlling for seasonality and geographic biases of the proxy data, simulate cooler 6 ka than preindustrial temperatures for most (80%) regions, with agreement for warming confined to the Arctic (Figure 8). Using the same metric for global agreement, 9 of 35 (26%) regions agree compared to 18 of 35 in disagreement (Figure 9b).

Comparing these results shows that the globally consistent proxy–model disagreement for mid-Holocene temperature, known as the Holocene Temperature Conundrum (Liu et al., 2014), is not observed for hydroclimate. The simulated precipitation pattern is more spatially varied, and regions with opposing signs are in closer proximity than for the temperature pattern (Figure 8). Spatial heterogeneity in the model simulations is also shown by more grid cells containing a mix of both dry and wet anomalies. Although some regions do have notable proxy–model precipitation disagreements, as discussed above for North America, for many others the proxy agreement is consistent with at least some model runs. Therefore, because models are more likely to simulate a range of wet and dry signals for the same locations, disagreements between the proxies and models are less systematically biased for hydroclimate than temperature. In this way, for the Holocene, proxy data and models agree better for hydroclimate than they do for temperature.

The level of proxy–model hydroclimate agreement is also significant relative to random; the likelihood of 19 regions agreeing is less than 1%. Furthermore, model uncertainty is insufficient to explain this level of hydroclimate agreement as a majority (13) of these regions indicate consensus (>60% in both data types) for wetter or dryer mid-Holocene anomalies. Thus, the proxy–model hydroclimate agreement is better than random and generally improves in regions where the climate signal is larger.

## 5. Summary and Conclusions

To investigate hydroclimate during the Holocene, we compiled a new multi-proxy data set to characterize relative changes in terrestrial net precipitation and effective moisture. Regional compilations of these proxy records provide a basis for understanding spatial patterns of changes in hydroclimate. We find coherent spatiotemporal patterns distinguishing the tropics and extratropics over the past 12 ka. Evidence from individual proxy records and model simulations suggest that the primary driver of hydroclimatic change was insolation and temperature-driven modulations of atmospheric circulation. As a result, long-term millennial-scale trends greatly exceed centennial-scale variability in Holocene hydroclimate, with many regions experiencing substantially different hydroclimatic conditions during the early Holocene relative to the last millennium.

Comparisons between proxy and model results demonstrate relatively similar overall patterns of Holocene hydroclimate evolution and, despite the well-documented challenges for reconstructing hydroclimate variability, we find better proxy–model agreement for precipitation than for temperature. This result is particularly true of tropical monsoon regions where greater magnitudes of change and a more direct climate response to insolation changes overcome local variability and uncertainty. In the midlatitudes, the direction of change is less clear. Most notable among these disagreements is the aridity identified by proxy records in regions of western North America during the early and mid-Holocene where model simulations show almost uniformly wetter conditions. At high latitudes, both proxy and model data indicate a strong positive covariance of moisture availability and temperature, consistent with theory and projections for increased precipitation in these regions with future warming.

Despite the challenges of quantifying hydroclimate variability, within many regions there is better consensus between proxy composites and model simulations than there is for temperature comparisons. For assessing transient trends, occurrences of proxy–model hydroclimate agreement is partially attributable to the more frequent dissimilarity between models of simulated precipitation as compared to temperature; the greater dispersion among simulations means that at least one model is likely to match the proxy composites. However, by evaluating

the sign of mid-Holocene anomalies, we show that proxy–model agreement for hydroclimate is robust, particularly where the climate signal is strong. This conclusion is somewhat surprising, as temperature changes are more spatially uniform than hydroclimate; however, the consistent disagreement between proxy and simulated Holocene temperatures has been well-described and consistently observed. Given the differing results between these climate variables, any systematic bias in proxy records or models simulations that cause the Holocene Temperature Conundrum cannot fully explain hydroclimate proxy–model disagreements.

The mid-Holocene may serve as a partial analogue for future hydroclimate change in part because polar amplification is a feature of both mid-Holocene and modern global warming. A warmer Arctic corresponds with both reduced ice sheet extent and a weak LTG, and results presented here demonstrate that spatial patterns of mid-Holocene warmth had global implications for atmospheric circulation and moisture dynamics including intensified monsoon circulation and greater aridity for midlatitude regions in the Northern Hemisphere. Unlike the early and mid-Holocene, when variations in radiative forcing were asymmetrical across northern and southern latitudes and seasons, future warming is projected in all regions and seasons, and the analogue starts to break down. Nevertheless, a better understanding of how long-term temperature changes influence hydroclimate is critical, and Holocene hydroclimate data provide an important benchmark for models used to simulate future changes.

### Conflict of Interest

The authors declare no conflicts of interest relevant to this study.

### Data Availability Statement

The hydroclimate proxy records used in the data compilation are available in LiPD format at [https://lipdverse.org/HoloceneHydroclimate/0\\_7\\_0/](https://lipdverse.org/HoloceneHydroclimate/0_7_0/). A summary table of the proxy data is provided at Hancock, McKay, Erb, Kaufman, and Routson (2023) and described by Table S1 in Supporting Information S1. The temperature proxy records compiled in Temp12k are from Kaufman, McKay, and Routson (2020). The TraCE-21ka simulation data are available at <https://www.earthsystemgrid.org/dataset/ucar.cgd.cesm.trace.html>. The HadCM3 simulations results used in this study are archived at Hancock, McKay, Erb, Kaufman, Routson, et al. (2023). Data for the CMIP6 simulations are available through data portals such as <https://esgf-node.llnl.gov/projects/cmip6/>, and a list of the specific CMIP6 simulations used by this study is provided by Table S2 in Supporting Information S1. Python and R notebooks used for data analysis and figure creation are available at <https://github.com/clhancock/HoloceneHydroclimate>. CSV files for the proxy composites, agreement statistics, and correlations coefficient results are also provided at this Github link and are archived with the notebooks at Hancock, McKay, Erb, Kaufman, Routson, et al. (2023). Data and software for analyzing the IPCC reference region data and software for analysis from Iturbide et al. (2021) and Hauser et al. (2022). Proxy records were analyzed using LiPD-utilities (Heiser et al., 2018), geoChronR (McKay et al., 2020), and compositeR (McKay & Hancock, 2023).

### References

- An, Z., Colman, S. M., Zhou, W., Li, X., Brown, E. T., Jull, A. J. T., et al. (2012). Interplay between the westerlies and Asian monsoon recorded in Lake Qinghai sediments since 32 ka. *Scientific Reports*, 2(1), 619. <https://doi.org/10.1038/srep00619>
- An, Z., Porter, S. C., Kutzbach, J. E., Wu, X. H., Wang, S. M., Liu, X. D., et al. (2000). Asynchronous Holocene optimum of the East Asian monsoon. *Quaternary Science Reviews*, 19(8), 743–762. [https://doi.org/10.1016/S0277-3791\(99\)00031-1](https://doi.org/10.1016/S0277-3791(99)00031-1)
- Asmerom, Y., Polyak, V., Burns, S., & Rasmussen, J. (2007). Solar forcing of Holocene climate: New insights from a speleothem record, southwestern United States. *Geology*, 35(1), 1–4. <https://doi.org/10.1130/G22865A.1>
- Bartlein, P. J., Anderson, K. H., Anderson, P. M., Edwards, M. E., Mock, C. J., Thompson, R. S., et al. (1998). Paleoclimate simulations for North America over the past 21,000 years: Features of the simulated climate and comparisons with paleoenvironmental data. *Quaternary Science Reviews*, 17(6–7), 549–585. [https://doi.org/10.1016/S0277-3791\(98\)00012-2](https://doi.org/10.1016/S0277-3791(98)00012-2)
- Bartlein, P. J., Webb, T., & Fleri, E. (1984). Holocene climatic change in the northern midwest: Pollen-derived estimates. *Quaternary Research*, 22(3), 361–374. [https://doi.org/10.1016/0033-5894\(84\)90029-2](https://doi.org/10.1016/0033-5894(84)90029-2)
- Berger, A., & Loutre, M. F. (1991). Insolation values for the climate of the last 10 million years. *Quaternary Science Reviews*, 10(4), 297–317. [https://doi.org/10.1016/0277-3791\(91\)90033-Q](https://doi.org/10.1016/0277-3791(91)90033-Q)
- Bernal, J. P., Cruz, F. W., Strikis, N. M., Wang, X., Deininger, M., Catunda, M. C. A., et al. (2016). High-resolution Holocene south American monsoon history recorded by a speleothem from Botuverá Cave, Brazil. *Earth and Planetary Science Letters*, 450, 186–196. <https://doi.org/10.1016/j.epsl.2016.06.008>
- Bintanja, R., & Selten, F. M. (2014). Future increases in Arctic precipitation linked to local evaporation and sea-ice retreat. *Nature*, 509(7501), 479–482. <https://doi.org/10.1038/nature13259>
- Brierley, C. M., Zhao, A., Harrison, S. P., Braconnot, P., Williams, C. J. R., Thornalley, D. J. R., et al. (2020). Large-scale features and evaluation of the PMIP4-CMIP6 midHolocene simulations. *Climate of the Past*, 16(5), 1847–1872. <https://doi.org/10.5194/cp-16-1847-2020>

### Acknowledgments

Funding for this research was provided by the U.S. National Science Foundation (AGS-1903465 and AGS-2002328). We thank the original data generators who made their data available for reuse and we acknowledge the data repositories for safeguarding these assets.

- Cai, Y., Tan, L., Cheng, H., An, Z., Edwards, R. L., Kelly, M. J., et al. (2010). The variation of summer monsoon precipitation in central China since the last deglaciation. *Earth and Planetary Science Letters*, 291(1), 21–31. <https://doi.org/10.1016/j.epsl.2009.12.039>
- Chase, B. M., Lim, S., Chevalier, M., Boom, A., Carr, A. S., Meadows, M. E., & Reimer, P. J. (2015). Influence of tropical easterlies in southern Africa's winter rainfall zone during the Holocene. *Quaternary Science Reviews*, 107, 138–148. <https://doi.org/10.1016/j.quascirev.2014.10.011>
- Cheng, H., Sinha, A., Wang, X., Cruz, F. W., & Edwards, R. L. (2012). The global paleomonsoon as seen through speleothem records from Asia and the Americas. *Climate Dynamics*, 39(5), 1045–1062. <https://doi.org/10.1007/s00382-012-1363-7>
- Cheng, J., Wu, H., Liu, Z., Gu, P., Wang, J., Zhao, C., et al. (2021). Vegetation feedback causes delayed ecosystem response to East Asian summer monsoon rainfall during the Holocene. *Nature Communications*, 12(1), 1843. <https://doi.org/10.1038/s41467-021-22087-2>
- Chevalier, M., Brewer, S., & Chase, B. M. (2017). Qualitative assessment of PMIP3 rainfall simulations across the eastern African monsoon domains during the mid-Holocene and the Last Glacial Maximum. *Quaternary Science Reviews*, 156, 107–120. <https://doi.org/10.1016/j.quascirev.2016.11.028>
- Chou, C., & Neelin, J. D. (2003). Mechanisms limiting the northward extent of the northern summer monsoons over North America, Asia, and Africa. *Journal of Climate*, 16(3), 406–425. [https://doi.org/10.1175/1520-0442\(2003\)016<0406:MLTNEO>2.0.CO;2](https://doi.org/10.1175/1520-0442(2003)016<0406:MLTNEO>2.0.CO;2)
- COHMAP Members (1988). Climatic changes of the last 18,000 years: Observations and model simulations. *Science*, 241(4869), 1043–1052. <https://doi.org/10.1126/science.241.4869.1043>
- Collins, W. D., Bitz, C. M., Blackmon, M. L., Bonan, G. B., Bretherton, C. S., Carton, J. A., et al. (2006). The community climate system model version 3 (CCSM3). *Journal of Climate*, 19(11), 2122–2143. <https://doi.org/10.1175/JCLI3761.1>
- Comas-Bru, L., Rehfeld, K., Roesch, C., Amirnezhad-Mozhdehi, S., Harrison, S. P., Atsawaranant, K., et al. (2020). SISALv2: A comprehensive speleothem isotope database with multiple age–depth models. *Earth System Science Data*, 12(4), 2579–2606. <https://doi.org/10.5194/essd-12-2579-2020>
- Commerford, J. L., Grimm, E. C., Morris, C. J., Nurse, A., Stefanova, I., & McLauchlan, K. K. (2018). Regional variation in Holocene climate quantified from pollen in the Great Plains of North America. *International Journal of Climatology*, 38(4), 1794–1807. <https://doi.org/10.1002/joc.5296>
- Davis, B. A. S., & Brewer, S. (2009). Orbital forcing and role of the latitudinal insolation/temperature gradient. *Climate Dynamics*, 32(2), 143–165. <https://doi.org/10.1007/s00382-008-0480-9>
- Deininger, M., McDermott, F., Cruz, F. W., Bernal, J. P., Mudelsee, M., Vohnhof, H., et al. (2020). Inter-hemispheric synchronicity of Holocene precipitation anomalies controlled by Earth's latitudinal insolation gradients. *Nature Communications*, 11(1), 5447. <https://doi.org/10.1038/s41467-020-19021-3>
- de Menocal, P., Ortiz, J., Guilderson, T., Adkins, J., Sarnthein, M., Baker, L., & Yarusinsky, M. (2000). Abrupt onset and termination of the African Humid Period. *Quaternary Science Reviews*, 19(1–5), 347–361. [https://doi.org/10.1016/S0277-3791\(99\)00081-5](https://doi.org/10.1016/S0277-3791(99)00081-5)
- Gomez, B., Carter, L., Trustrum, N. A., Page, M. J., & Orpin, A. R. (2013). Coherent rainfall response to middle- and late-Holocene climate variability across the mid-latitude South Pacific. *The Holocene*, 23(7), 1002–1007. <https://doi.org/10.1177/0959683613479679>
- Hancock, C., McKay, N., Erb, M., Kaufman, D., & Routson, C. (2023). Summary Table for Holocene Hydroclimate Dataset (Hancock et al., 2023) [Dataset]. Figshare. <https://doi.org/10.6084/m9.figshare.22814366.v2>
- Hancock, C., McKay, N., Erb, M., Kaufman, D., Routson, C., Ivanovic, R., et al. (2023). clhancock/HoloceneHydroclimate: HoloceneHydroclimate\_v0.1.0 [Dataset]. Zenodo. <https://doi.org/10.5281/zenodo.7939488>
- Harrison, S. P., Bartlein, P. J., Brewer, S., Prentice, I. C., Boyd, M., Hessler, I., et al. (2014). Climate model benchmarking with glacial and mid-Holocene climates. *Climate Dynamics*, 43(3), 671–688. <https://doi.org/10.1007/s00382-013-1922-6>
- Hauser, M., Spring, A., Busecke, J., Driel, M. V., Lorenz, R., & readthedocs-assistant. (2022). mathause/regionmask: Version 0.9.0 [Software]. Zenodo. <https://doi.org/10.5281/zenodo.3992368>
- He, F. (2011). *Simulating transient climate evolution of the last deglaciation with CCSM3 (PhD)*. University of Wisconsin-Madison.
- Heiser, C., McKay, N., Simpson, G., & Routson, C. (2018). nickmckay/LiPD-utilities: Version 0.2.5.5 [Software]. Zenodo. <https://doi.org/10.5281/zenodo.1256889>
- Hermann, N. W., Oster, J. L., & Ibarra, D. E. (2018). Spatial patterns and driving mechanisms of mid-Holocene hydroclimate in western North America. *Journal of Quaternary Science*, 33(4), 421–434. <https://doi.org/10.1002/jqs.3023>
- Herzschuh, U., Böhmert, T., Li, C., Cao, X., Hébert, R., Dallmeyer, A., et al. (2022). Reversals in temperature-precipitation correlations in the northern hemisphere extratropics during the Holocene. *Geophysical Research Letters*, 49(22), e2022GL099730. <https://doi.org/10.1029/2022GL099730>
- Herzschuh, U., Böhmert, T., Li, C., Chevalier, M., Hébert, R., Dallmeyer, A., et al. (2023). LegacyClimate 1.0: A dataset of pollen-based climate reconstructions from 2594 northern hemisphere sites covering the last 30kyr and beyond. *Earth System Science Data Discussions*, 15(6), 2235–2258. <https://doi.org/10.5194/essd-15-2235-2023>
- Iturbide, M., Gutierrez, J. M., Alvarez, E. C., Bedia, J., Hauser, M., & Manzanar, R. (2021). SantanderMetGroup/ATLAS: Final version of "IPCC WGI reference regions v4" v2.0. [Dataset]. Zenodo. <https://doi.org/10.5281/zenodo.3998463>
- Iturbide, M., Gutiérrez, J. M., Alves, L. M., Bedia, J., Cerezo-Mota, R., Gimadevilla, E., et al. (2020). An update of IPCC climate reference regions for subcontinental analysis of climate model data: Definition and aggregated datasets. *Earth System Science Data*, 12(4), 2959–2970. <https://doi.org/10.5194/essd-12-2959-2020>
- Ivanovic, R. F., Gregoire, L. J., Kageyama, M., Roche, D. M., Valdes, P. J., Burke, A., et al. (2016). Transient climate simulations of the deglaciation 21–9 thousand years before present (version 1) – PMIP4 Core experiment design and boundary conditions. *Geoscientific Model Development*, 9(7), 2563–2587. <https://doi.org/10.5194/gmd-9-2563-2016>
- Jaeschke, A., Rühlemann, C., Arz, H., Heil, G., & Lohmann, G. (2007). Coupling of millennial-scale changes in sea surface temperature and precipitation off northeastern Brazil with high-latitude climate shifts during the last glacial period. *Paleoceanography*, 22(4), PA4206. <https://doi.org/10.1029/2006PA001391>
- Jiang, D., Tian, Z., & Lang, X. (2015). Mid-Holocene global monsoon area and precipitation from PMIP simulations. *Climate Dynamics*, 44(9), 2493–2512. <https://doi.org/10.1007/s00382-014-2175-8>
- Jin, L., Schneider, B., Park, W., Latif, M., Khon, V., & Zhang, X. (2014). The spatial-temporal patterns of Asian summer monsoon precipitation in response to Holocene insolation change: A model-data synthesis. *Quaternary Science Reviews*, 85, 47–62. <https://doi.org/10.1016/j.quascirev.2013.11.004>
- Kaufman, D., McKay, N., Routson, C., Erb, M., Dätwyler, C., Sommer, P. S., et al. (2020). Holocene global mean surface temperature, a multi-method reconstruction approach. *Scientific Data*, 7(1), 201. <https://doi.org/10.1038/s41597-020-0530-7>
- Kaufman, D., McKay, N., Routson, C., Erb, M., Davis, B., Heiri, O., et al. (2020). A global database of Holocene paleotemperature records. *Scientific Data*, 7(1), 115. <https://doi.org/10.1038/s41597-020-0445-3>

- Kaufman, D. S., McKay, N. P., & Routson, C. (2020). NOAA/WDS paleoclimatology – Temperature 12k database [Dataset]. NOAA National Centers for Environmental Information. <https://doi.org/10.25921/4ry2-g808>
- Konecky, B. L., McKay, N. P., Churakova (Sidorova), O. V., Comas-Bru, L., Dassié, E. P., DeLong, K. L., et al. (2020). The Iso2k database: A global compilation of paleo- $\delta^{18}\text{O}$  and  $\delta^2\text{H}$  records to aid understanding of common era climate. *Earth System Science Data*, *12*(3), 2261–2288. <https://doi.org/10.5194/essd-12-2261-2020>
- Kong, W., & Chiang, J. C. H. (2020). Interaction of the westerlies with the Tibetan plateau in determining the Mei-Yu termination. *Journal of Climate*, *33*(1), 339–363. <https://doi.org/10.1175/JCLI-D-19-0319.1>
- Krause, C. E., Gagan, M. K., Dunbar, G. B., Hantoro, W. S., Hellstrom, J. C., Cheng, H., et al. (2019). Spatio-temporal evolution of Australasian monsoon hydroclimate over the last 40,000 years. *Earth and Planetary Science Letters*, *513*, 103–112. <https://doi.org/10.1016/j.epsl.2019.01.045>
- Lamy, F., Kilian, R., Arz, H. W., Francois, J.-P., Kaiser, J., Prange, M., & Steinke, T. (2010). Holocene changes in the position and intensity of the southern westerly wind belt. *Nature Geoscience*, *3*(10), 695–699. <https://doi.org/10.1038/ngeo959>
- Lézine, A.-M., Hély, C., Grenier, C., Braconnot, P., & Krinner, G. (2011). Sahara and Sahel vulnerability to climate changes, lessons from Holocene hydrological data. *Quaternary Science Reviews*, *30*(21), 3001–3012. <https://doi.org/10.1016/j.quascirev.2011.07.006>
- Liefert, D. T., & Shuman, B. N. (2020). Pervasive desiccation of North American lakes during the late quaternary. *Geophysical Research Letters*, *47*(3), e2019GL086412. <https://doi.org/10.1029/2019GL086412>
- Lin, Y., Ramstein, G., Wu, H., Rani, R., Braconnot, P., Kageyama, M., et al. (2019). Mid-Holocene climate change over China: Model-data discrepancy. *Climate of the Past*, *15*(4), 1223–1249. <https://doi.org/10.5194/cp-15-1223-2019>
- Liu, Z., Zhu, J., Rosenthal, Y., Zhang, X., Otto-Bliesner, B. L., Timmermann, A., et al. (2014). The Holocene temperature conundrum. *Proceedings of the National Academy of Sciences*, *111*(34), E3501–E3505. <https://doi.org/10.1073/pnas.1407229111>
- Lu, F., Ma, C., Zhu, C., Lu, H., Zhang, X., Huang, K., et al. (2019). Variability of East Asian summer monsoon precipitation during the Holocene and possible forcing mechanisms. *Climate Dynamics*, *52*(1), 969–989. <https://doi.org/10.1007/s00382-018-4175-6>
- Marcott, S. A., Shakun, J. D., Clark, P. U., & Mix, A. C. (2013). A reconstruction of regional and global temperature for the past 11,300 Years. *Science*, *339*(6124), 1198–1201. <https://doi.org/10.1126/science.1228026>
- Martin, H., Schmid, C., Knitter, D., & Tietze, C. (2021). oxcAAR: interface to “OxCal” radiocarbon calibration (Version 1.1.1). Retrieved from <https://CRAN.R-project.org/package=oxcAAR>
- Mauri, A., Davis, B. A. S., Collins, P. M., & Kaplan, J. O. (2014). The influence of atmospheric circulation on the mid-Holocene climate of Europe: A data–model comparison. *Climate of the Past*, *10*(5), 1925–1938. <https://doi.org/10.5194/cp-10-1925-2014>
- McCrystall, M. R., Stroeve, J., Serreze, M., Forbes, B. C., & Screen, J. A. (2021). New climate models reveal faster and larger increases in Arctic precipitation than previously projected. *Nature Communications*, *12*(1), 6765. <https://doi.org/10.1038/s41467-021-27031-y>
- McKay, N., Emile-Geay, J., Khider, D., & Heiser, C. (2020). nickmckay/GeoChronR: May 2020 pre-release version 1.1.0-beta [Software]. Zenodo. <https://doi.org/10.5281/zenodo.3834799>
- McKay, N., & Hancock, C. (2023). nickmckay/compositeR: V0.1.0 [Software]. Zenodo. <https://doi.org/10.5281/zenodo.7951515>
- McKay, N. P., & Emile-Geay, J. (2016). Technical note: The linked paleo data framework – A common tongue for paleoclimatology. *Climate of the Past*, *12*(4), 1093–1100. <https://doi.org/10.5194/cp-12-1093-2016>
- McKay, N. P., Emile-Geay, J., & Khider, D. (2021). geoChronR – An R package to model, analyze, and visualize age-uncertain data. *Geochronology*, *3*(1), 149–169. <https://doi.org/10.5194/gchron-3-149-2021>
- Mollier-Vogel, E., Leduc, G., Bösch, T., Martinez, P., & Schneider, R. R. (2013). Rainfall response to orbital and millennial forcing in northern Peru over the last 18 ka. *Quaternary Science Reviews*, *76*, 29–38. <https://doi.org/10.1016/j.quascirev.2013.06.021>
- Morrill, C., Meador, E., Livneh, B., Liefert, D. T., & Shuman, B. N. (2019). Quantitative model-data comparison of mid-Holocene lake-level change in the central Rocky Mountains. *Climate Dynamics*, *53*(1–2), 1077–1094. <https://doi.org/10.1007/s00382-019-04633-3>
- Ning, L., Liu, J., Bradley, R. S., & Yan, M. (2019). Comparing the spatial patterns of climate change in the 9th and 5th millennia BP from TRACE-21 model simulations. *Climate of the Past*, *15*(1), 41–52. <https://doi.org/10.5194/cp-15-41-2019>
- Osman, M. B., Tierney, J. E., Zhu, J., Tardif, R., Hakim, G. J., King, J., & Poulsen, C. J. (2021). Globally resolved surface temperatures since the last glacial maximum. *Nature*, *599*(7884), 239–244. <https://doi.org/10.1038/s41586-021-03984-4>
- Rees, A. B. H., Cwynar, L. C., & Fletcher, M.-S. (2015). Southern westerly winds submit to the ENSO regime: A multiproxy paleohydrology record from lake Dobson, Tasmania. *Quaternary Science Reviews*, *126*, 254–263. <https://doi.org/10.1016/j.quascirev.2015.08.022>
- Reimer, P. J., Austin, W. E. N., Bard, E., Bayliss, A., Blackwell, P. G., Ramsey, C. B., et al. (2020). The IntCal20 Northern Hemisphere radiocarbon age calibration curve (0–55 cal kBP). *Radiocarbon*, *62*(4), 725–757. <https://doi.org/10.1017/RDC.2020.41>
- Routson, C. C., Kaufman, D. S., McKay, N. P., Erb, M. P., Arcusa, S. H., Brown, K. J., et al. (2021). A multiproxy database of western North American Holocene paleoclimate records. *Earth System Science Data*, *13*(4), 1613–1632. <https://doi.org/10.5194/essd-13-1613-2021>
- Routson, C. C., McKay, N. P., Kaufman, D. S., Erb, M. P., Gooose, H., Shuman, B. N., et al. (2019). Mid-latitude net precipitation decreased with Arctic warming during the Holocene. *Nature*, *568*(7750), 83–87. <https://doi.org/10.1038/s41586-019-1060-3>
- Shepherd, T. G. (2014). Atmospheric circulation as a source of uncertainty in climate change projections. *Nature Geoscience*, *7*(10), 703–708. <https://doi.org/10.1038/ngeo2253>
- Shi, J., & Yan, Q. (2019). Evolution of the Asian–African monsoonal precipitation over the last 21 kyr and the associated dynamic mechanisms. *Journal of Climate*, *32*(19), 6551–6569. <https://doi.org/10.1175/JCLI-D-19-0074.1>
- Shuman, B. N., & Marsicek, J. (2016). The structure of Holocene climate change in mid-latitude North America. *Quaternary Science Reviews*, *141*, 38–51. <https://doi.org/10.1016/j.quascirev.2016.03.009>
- Street-Perrott, F. A., Marchand, D. S., Roberts, N., & Harrison, S. P. (1989). *Global lake-level variations from 18,000 to 0 years ago: A palaeoclimatic analysis*. Geography School. No. DOE/ER/60304-H1. <https://doi.org/10.2172/5609291>
- Sundqvist, H. S., Kaufman, D. S., McKay, N. P., Balascio, N. L., Briner, J. P., Cwynar, L. C., et al. (2014). Arctic Holocene proxy climate database - New approaches to assessing geochronological accuracy and encoding climate variables. *Climate of the Past*, *10*(4), 1605–1631. <https://doi.org/10.5194/cp-10-1605-2014>
- Tarasov, P. E., Webb, T., III, Andreev, A. A., Afanas'eva, N. B., Berezina, N. A., Bezusko, L. G., et al. (1998). Present-day and mid-Holocene biomes reconstructed from pollen and plant macrofossil data from the former Soviet Union and Mongolia. *Journal of Biogeography*, *25*(6), 1029–1053. <https://doi.org/10.1046/j.1365-2699.1998.00236.x>
- Tierney, J. E., & de Menocal, P. B. (2013). Abrupt shifts in horn of Africa hydroclimate since the last glacial maximum. *Science*, *342*(6160), 843–846. <https://doi.org/10.1126/science.1240411>
- Tierney, J. E., Pausata, F. S. R., & de Menocal, P. B. (2017). Rainfall regimes of the green Sahara. *Science Advances*, *3*(1), e1601503. <https://doi.org/10.1126/sciadv.1601503>

- Voigt, I., Chiessi, C. M., Prange, M., Multiza, S., Groeneveld, J., Varma, V., & Henrich, R. (2015). Holocene shifts of the southern westerlies across the South Atlantic. *Paleoceanography*, *30*(2), 39–51. <https://doi.org/10.1002/2014PA002677>
- Williams, J. W., Shuman, B., Bartlein, P. J., Diffenbaugh, N. S., & Webb, T. (2010). Rapid, time-transgressive, and variable responses to early Holocene midcontinental drying in North America. *Geology*, *38*(2), 135–138. <https://doi.org/10.1130/G30413.1>
- Zhang, X., Jin, L., Chen, J., Chen, F., Park, W., Schneider, B., & Latif, M. (2017). Detecting the relationship between moisture changes in arid central Asia and East Asia during the Holocene by model-proxy comparison. *Quaternary Science Reviews*, *176*, 36–50. <https://doi.org/10.1016/j.quascirev.2017.09.012>
- Zhang, X., Jin, L., Huang, W., & Chen, F. (2016). Forcing mechanisms of orbital-scale changes in winter rainfall over northwestern China during the Holocene. *The Holocene*, *26*(4), 549–555. <https://doi.org/10.1177/0959683615612569>
- Zhao, Y., & Harrison, S. P. (2012). Mid-Holocene monsoons: A multi-model analysis of the inter-hemispheric differences in the responses to orbital forcing and ocean feedbacks. *Climate Dynamics*, *39*(6), 1457–1487. <https://doi.org/10.1007/s00382-011-1193-z>
- Zhou, P., Shi, Z., Li, X., & Zhou, W. (2020). Response of westerly jet over the Northern Hemisphere to astronomical insolation during the Holocene. *Frontiers of Earth Science*, *8*, 282. <https://doi.org/10.3389/feart.2020.00282>
- Zhuang, J., Dussin, R., Jüling, A., & Rasp, S. (2020). xESMF: V0.3.0 [Software]. Zenodo. <https://doi.org/10.5281/zenodo.3700105>

## References From the Supporting Information

- Boucher, O., Servonnat, J., Albright, A. L., Aumont, O., Balkanski, Y., Bastrikov, V., et al. (2020). Presentation and evaluation of the IPSL-CM6A-LR climate model. *Journal of Advances in Modeling Earth Systems*, *12*(7), e2019MS002010. <https://doi.org/10.1029/2019MS002010>
- Gettelman, A., Hannay, C., Bacmeister, J. T., Neale, R. B., Pendergrass, A. G., Danabasoglu, G., et al. (2019). High climate sensitivity in the community Earth system model version 2 (CESM2). *Geophysical Research Letters*, *46*(14), 8329–8337. <https://doi.org/10.1029/2019GL083978>
- Guo, C., Bentsen, M., Bethke, I., Ilicak, M., Tjiputra, J., Toniazzi, T., et al. (2019). Description and evaluation of NorESM1-F: A fast version of the Norwegian Earth system model (NorESM). *Geoscientific Model Development*, *12*(1), 343–362. <https://doi.org/10.5194/gmd-12-343-2019>
- Hajima, T., Watanabe, M., Yamamoto, A., Tatebe, H., Noguchi, M. A., Abe, M., et al. (2020). Development of the MIROC-ES2L Earth system model and the evaluation of biogeochemical processes and feedbacks. *Geoscientific Model Development*, *13*(5), 2197–2244. <https://doi.org/10.5194/gmd-13-2197-2020>
- Kelley, M., Schmidt, G. A., Nazarenko, L. S., Bauer, S. E., Ruedy, R., Russell, G. L., et al. (2020). GISS-E2.1: Configurations and climatology. *Journal of Advances in Modeling Earth Systems*, *12*(8), e2019MS002025. <https://doi.org/10.1029/2019MS002025>
- Li, L., Yu, Y., Tang, Y., Lin, P., Xie, J., Song, M., et al. (2020). The flexible global ocean-atmosphere-land system model grid-point version 3 (FGOALS-g3): Description and evaluation. *Journal of Advances in Modeling Earth Systems*, *12*(9), e2019MS002012. <https://doi.org/10.1029/2019MS002012>
- Mauritsen, T., Bader, J., Becker, T., Behrens, J., Bittner, M., Brokopf, R., et al. (2019). Developments in the MPI-M Earth system model version 1.2 (MPI-ESM1.2) and its response to increasing CO<sub>2</sub>. *Journal of Advances in Modeling Earth Systems*, *11*(4), 998–1038. <https://doi.org/10.1029/2018MS001400>
- Sidorenko, D., Rackow, T., Jung, T., Semmler, T., Barbi, D., Danilov, S., et al. (2015). Towards multi-resolution global climate modeling with ECHAM6-FESOM. Part I: Model formulation and mean climate. *Climate Dynamics*, *44*(3), 757–780. <https://doi.org/10.1007/s00382-014-2290-6>
- Volodin, E. M., Mortikov, E. V., Kostyrkin, S. V., Galin, V. Y., Lykossov, V. N., Gritsun, A. S., et al. (2018). Simulation of the modern climate using the INM-CM48 climate model. *Russian Journal of Numerical Analysis and Mathematical Modelling*, *33*(6), 367–374. <https://doi.org/10.1515/rnam-2018-0032>
- Wang, H., Li, L., Chen, X., & Wang, B. (2022). Evaluating the nature and extent of changes to climate sensitivity between FGOALS-g2 and FGOALS-g3. *Journal of Geophysical Research: Atmospheres*, *127*(3), e2021JD035852. <https://doi.org/10.1029/2021JD035852>
- Wyser, K., van Noije, T., Yang, S., von Hardenberg, J., O'Donnell, D., & Döschner, R. (2020). On the increased climate sensitivity in the EC-Earth model from CMIP5 to CMIP6. *Geoscientific Model Development*, *13*(8), 3465–3474. <https://doi.org/10.5194/gmd-13-3465-2020>
- Yukimoto, S., Kawai, H., Koshiro, T., Oshima, N., Yoshida, K., Urakawa, S., et al. (2019). The meteorological research institute Earth system model version 2.0, MRI-ESM2.0: Description and basic evaluation of the physical component. *Journal of the Meteorological Society of Japan. Ser. II*, *97*(5), 931–965. <https://doi.org/10.2151/jmsj.2019-051>